Available online at www.sciencedirect.com
SCIENCE DIRECT®
Thermochimica Acta 403 (2003) 137–151
thermochimica acta
www.elsevier.com/locate/tca

Extended least-squares analysis of heat capacities incorporating the effect of phase transitions and its application to the deuteration-induced phase transition in $Rb_3D(SO_4)_2$ ☆

Takasuke Matsuo [a,*], Nobuki Tanaka [a], Mari Fukai [a], Osamu Yamamuro [a], Akira Inaba [a], Mizuhiko Ichikawa [b]

[a] *Department of Chemistry, Graduate School of Science, Osaka University, Machikaneyama-Cho 1-1, Toyonaka 560-0043, Japan*
[b] *Division of Physics, Graduate School of Science, Hokkaodo University, Sapporo 060-0810, Japan*

Received 31 July 2002; received in revised form 10 January 2003; accepted 17 January 2003

Abstract

A non-linear least-squares method of analysis has been developed for the heat capacities of solids undergoing phase transitions. It utilizes harmonic heat capacity functions corrected for thermal expansion. The unique feature of the method is that it incorporates the effect of a gradual phase transition in the fitting function for the low temperature phase. Compact expressions approximating the Debye function and the Ising model heat capacity function have been derived and presented in practical forms for use in the Kaleidagraph software. The method has been tested on the heat capacity of sodium chloride (which lacks a phase transition) and tri-rubidium deuterium disulfate ($Rb_3D(SO_4)_2$, TRDS) which undergoes a phase transition at 78.5 K in the deuterated form but not in the normal hydrogenous form. The excess entropy based on the fitting was 5.27 J K^{-1} mol^{-1}, close enough to $R \ln 2 = 5.76$ J K^{-1} mol^{-1} to suggest an order–disorder mechanism for the phase transition.

Keywords: Heat capacity; Excess heat capacity; Transition; Entropy; $Rb_3H(SO_4)_2$; NaCl

1. Introduction

In the past decade, commercial low temperature calorimeters have become available for accurate measurement of heat capacities that were previously attained only by calorimetric specialists employing specialized instruments. Newly available apparatuses produce high quality data that appear to allow meaningful analysis based on statistical mechanical theories, giving us crucial knowledge about the mechanism of the transition. In the analysis of heat capacity data of solids, it has been standard practice to separate the experimental data into normal and anomalous parts on various assumptions about their temperature dependence. The normal component is usually known qualitatively at least and is of a secondary interest, while determination of the anomalous part is the primary objective of the entire experimental work. Sometimes, it also happens that the normal part arises from a physically complicated mechanism but may be assumed to be a slowly varying function of temperature for which a polynomial in temperature is an adequate representation. Most often, the anomalous part is an excess heat capacity due to a phase transition while

☆ Contribution no. 77 from Research Center for Molecular Thermodynamics.

* Corresponding author. Tel.: +81-6-6850-5396; fax: +81-6-6850-5397.
E-mail address: matsuo@chem.sci.osaka-u.ac.jp (T. Matsuo).

0040-6031/03/$ – see front matter © 2003 Elsevier Science B.V. All rights reserved.
doi:10.1016/S0040-6031(03)00150-3

the normal part is the lattice heat capacity. Since the effect of a phase transition is usually confined within a limited interval of temperature, the standard procedure is to interpolate the normal heat capacities into the transition interval and subtract the interpolated curve from the experimental values to determine the excess heat capacity. Though this type of analysis is practical and often gives a reasonable result, one has to tolerate a certain degree of arbitrariness in the choice of the transition interval and the interpolation function. The Debye and Einstein heat capacity functions are standard ingredients of the interpolation function and optimized by non-linear fitting [1].

We have devised a least-squares interpolation scheme that includes the effect of phase transitions in the interpolation function. In this scheme, the experimental data to which the model function is fitted may contain the excess contribution to an unspecified proportion. The best-fit combination of the normal and excess parts is achieved by the least-squares optimization. Once the best-fit function is determined, the normal part is subtracted from the whole experimental data to determine the excess part. This greatly diminishes the arbitrariness in the interpolation. The original version of the fitting program was written in BASIC and has been used on various experimental data [2,3].

In the present paper, we describe a recent version of the fitting program based on more recent commercial software for numerical analysis. We use Kaleidagraph (version 3.51) for the actual calculation and graphic presentation. Other numerical analysis software will also be appropriate for the present purpose. The revised version of the fitting program may be useful in conjunction with computerized calorimeters now available commercially. It should be pointed out that, unlike the modulated DSC, adiabatic calorimetry with which we are concerned in this paper gives only static heat capacity. Hence, it is not necessary to consider complex values of the heat capacity.

Tri-rubidium deuterium disulfate ($Rb_3D(SO_4)_2$, TRDS) undergoes a phase transition at 78.5 K [4]. This phase transition is unusual in that it does not occur in tri-rubidium hydrogen disulfate ($Rb_3H(SO_4)_2$, TRHS). This strong isotope effect indicates the importance of the quantum nature of the motion of protons in determining even macroscopic properties of some crystals. The excess heat capacity of this compound is significant over a wide temperature range covering the transition temperature and this makes the evaluation of the transition entropy susceptible to various arbitrary factors mentioned above. The difficulty is especially great in this compound because the phonon heat capacity changes three- to fourfold in the temperature interval in question. We also recognize that the mean-field approximation described below is accurate for such a gradual transition [5]. We have applied the extended least-squares method to this phase transition and determined the excess heat capacity and entropy. We also present the analysis of the heat capacity of sodium chloride which we performed as a check of the non-linear least-squares analysis. Sodium chloride is available in high purity but only a limited set of heat capacity data has been published [6,7]. We measured the heat capacity of a single crystal of sodium chloride for T between 5 and 320 K.

2. The extended least-squares fitting

2.1. The principle of the method

Suppose that the normal heat capacity can be represented by harmonic oscillator heat capacity functions such as Debye and Einstein functions. In the previous method, we optimized the Debye and Einstein temperatures by fitting the heat capacity functions to experimental data outside the transition interval [2]. This works well in some cases and does not in others. The difficulty arises for phase transitions for which the excess heat capacities start to increase gradually far below the transition temperature. For such phase transitions, one cannot decide a unique temperature below which the effect of the transition is negligible. This difficulty has been coped with sometimes successfully by changing the temperature interval taken into the fitting [1,8]. In the extended fitting described here, we add a function of temperature to represent the phase transition for temperatures below the transition temperature. The interpolation function consists of two pieces, one for the high temperature region and the other for the low temperature region. The whole interpolation function is optimized against the experimental data. There is a gap between the temperature regions for the high and low temperature sets of data. The gap portion of the data is “masked” where the excess heat

capacity cannot be represented in a general parameterized form. The experimental data should cover the low temperature region where the excess contribution is significant. The function to be optimized is discontinuous at the transition temperature, but this does not cause difficulty.

In the fitting we may assign weights to the experimental data depending on the temperature. However, since there is no general way for weighting, we give a uniform weight in the following.

2.2. The excess heat capacity function

The entire experimental heat capacity of an actual phase transition is a complicated function of temperature. It varies from a transition to another depending on the underlying physical mechanism as well as on secondary effects such as purity of the sample. We cannot hope to find a mathematical function that reproduce the entire heat capacities of phase transitions in a general way. However, we need for the present purpose only a theoretical expression of the excess heat capacity at low temperature. The most generally applicable model is the Ising model. We solved it by mean-field approximation and gave the resulting heat capacity in a compact form [2]:

$$\begin{aligned}\text{Ising}\left(\frac{T_c}{T}\right) = {} & 6.311\exp\left(-1.390\frac{T_c}{T}\right) \\ & - 5.042\exp\left(-2\times 1.390\frac{T_c}{T}\right) \\ & + 18.70\exp\left(-3\times 1.390\frac{T_c}{T}\right). \qquad (1)\end{aligned}$$

This function multiplied by the molar gas constant $R = 8.3145\,\mathrm{J\,K^{-1}\,mol^{-1}}$ gives the heat capacity of the Ising model in the mean-field approximation, where T_c is the transition temperature. For temperatures above T_c, the function is assigned with a zero value. The function is reproduced in Fig. 1.

Although the Ising model is limited in various ways, the heat capacity due to thermal excitations across an energy gap is described well by this model at low temperature. The transition temperature is the only adjustable parameter in this part of the fitting function. A multiplicative factor to the Ising heat capacity may be included in the least-squares parameter, but often one can give a constant value (e.g. 1, 2, etc.) based

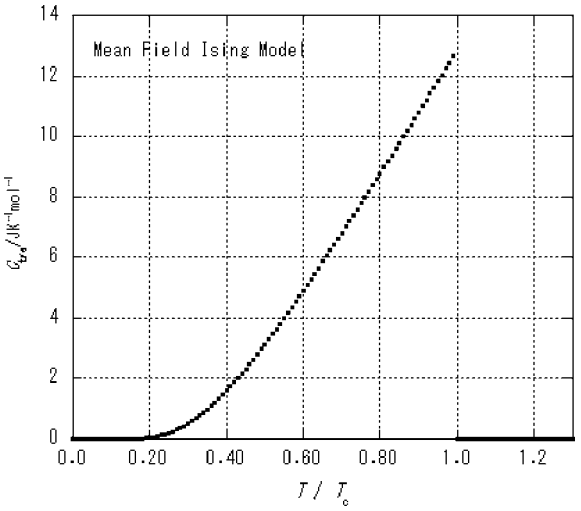

Fig. 1. The heat capacity of the Ising model solved in the mean-field approximation.

on the underlying model of the phase transition. The function given above does not describe the behavior of the heat capacity near the transition temperature. But it does not cause a difficulty since we use the function only for low temperature behavior of the excess heat capacity. Often phase transitions of the first order have a gradual portion below the transition temperature. This is also described well by Eq. (1).

One can also use any other parameterized functions to describe the excess heat capacity. The Schottky anomaly is one of the often-used anomalous parts. In fact, the mean-field calculation (Eq. (1)) is equivalent to the Schottky model in the low temperature limit and is an extension of the latter to higher temperatures. An extra part may also be added to the fitting function for the high temperature region. The fitting can be further generalized to admit three or more separate temperature regions each of which has different fitting function. The obvious limitation is set by the least-squares optimization routine. In our case, Kaleidagraph is capable of dealing with up to nine parameters.

2.3. Vibrational heat capacity functions

A sum of the Einstein and Debye functions are used to represent the vibrational heat capacity. The number of the functions depends on the number of vibrational degrees of freedom of the sample, the number of

characteristic temperatures known from spectroscopy, and on how the unknown characteristic vibrations are grouped together. For those vibrations whose frequencies are known from spectroscopic data, the Einstein functions of appropriate characteristic temperatures, weighted by the number of the vibrational modes, are included in the fitting function. The Einstein function is used in the form normalized to 1 at high temperature:

$$\mathrm{Ein}(\Theta_\mathrm{E}, T) = \frac{(\Theta_\mathrm{E}/T)^2 \exp(-\Theta_\mathrm{E}/T)}{(1-\exp(-\Theta_\mathrm{E}/T))^2}. \quad (2)$$

The Debye function cannot be written in a closed form of functions available in Kaleidagraph. We approximated it in three forms each appropriate for different inverse normalized temperatures (Θ_D/T). They are given in Appendix A.

Correction for the $C_p - C_v$ difference is approximated by ATC_v^2 in the interpolation function. The entire fitting function is as follows:

- For the high temperature region:

$$C_{p_\mathrm{H}}(T) = C_{vk}([\Theta_k], T) + C_{vu}([\Theta_u], T) + AT(C_{vk}([\Theta_k], T) + C_{vu}([\Theta_u], T))^2. \quad (3)$$

- For the low temperature region:

$$C_{p_\mathrm{L}}(T) = C_{p_\mathrm{H}}(T) + R\,\mathrm{Ising}(T_\mathrm{c}, T). \quad (4)$$

$C_{vk}([\Theta_k], T)$ is the sum of the Einstein heat capacity functions whose characteristic temperatures $[\Theta_k]$ are known from other sources such as spectroscopy. It may also contain a Debye term if the Debye temperature is known. Though it is not written explicitly, the function can include any other known contributions given in a calculable form.

$C_{vu}([\Theta_u], T)$ is the sum of the Debye and Einstein functions whose characteristic temperatures are not known. The set $[\Theta_u]$ of the characteristic temperatures contains Debye and Einstein temperatures to be optimized by the least-squares fitting. The $C_p - C_v$ correction coefficient A may be known from thermal expansion and compressibility data, in which case A should be assigned the constant value and excluded from the fitting parameters. More often, A is included in the fitting parameter. Finally the Ising term is added for the low temperature part of the fitting function, with the transition temperature included in the fitting parameters.

2.4. General polynomial interpolation functions

If the harmonic approximation by Debye and Einstein functions with a correction for the $C_p - C_v$ difference is found inappropriate for some reason, one can still use the extended fitting by taking a polynomial in T as the normal heat capacity function. In actual calculations, a low degree polynomial (e.g. of the third order) in temperature normalized to $+1$ or -1 in the temperature interval of fitting will be convenient.

3. Application to sodium chloride

The heat capacity of sodium chloride was measured between 5 and 320 K using a single crystal sample. The calorimeter used and the experimental procedure are the same as with $Rb_3D(SO_4)_2$ described below.

NaCl is a diatomic ionic crystal so that the Debye approximation will be appropriate at low energies, with a more localized density of states at higher energies near the Debye temperature. Three-parameter fit with a Debye function of weight 3, an Einstein function of weight 3 and the $C_p - C_v$ correction term was satisfactory for most of the temperatures. The final χ^2 value was 1.13 $(\mathrm{J\,K^{-1}\,mol^{-1}})^2$ for 152 points between 5.5 and 320 K. Here χ^2 is defined as the sum over dataset of the squares of the difference between the experimental and calculated heat capacities. The Debye and Einstein temperatures were 217.6 (0.5) and 260.5 (0.5) K, respectively, with the probable errors in the parentheses. The $C_p - C_v$ correction coefficient A was 3.72 (0.03) $\times 10^{-6}$ mol $\mathrm{J^{-1}}$. There were some systematic differences between the experiment and the fitted curve. A significantly better fitting was obtained with a five-parameter model function consisting of two Debye functions (weights 2 and 1), two Einstein functions (weights 2 and 1) and a $C_p - C_v$ term. The best-fit result was the Debye temperatures 321.8 (2.3) and 186.1 (1.1) K, Einstein temperatures 250.2 (1.5) and 154.9 (0.7) K and $A = 3.842\ (0.007) \times 10^{-6}$ mol $\mathrm{J^{-1}}$. χ^2 obtained was 0.0350 $(\mathrm{J\,K^{-1}\,mol^{-1}})^2$ for the same set of data. The result is shown in Fig. 2 and given in Table 1.

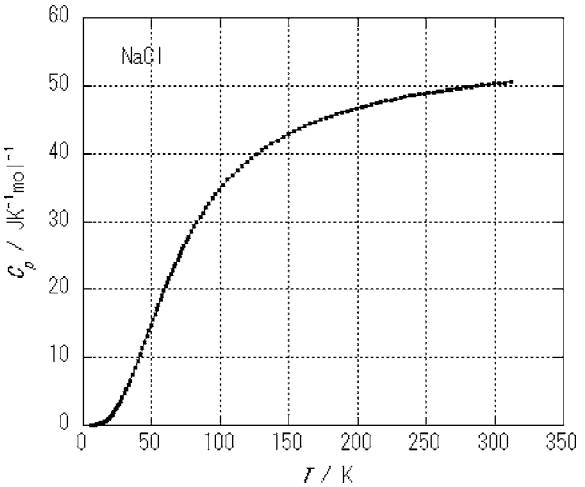

Fig. 2. The heat capacity of sodium chloride compared with the near-perfect five-parameter fit.

The coefficient A is correlated only weakly with other parameters, so that the best-fit value was accurate, even though it represents a small correction term (about 5% of the experimental C_p at 300 K). The $C_p - C_v$ difference from the fitting is equal to 2.55 J K^{-1} mol^{-1} at 293 K. The same quantity calculated from the bulk modulus 24.0 GPa and volume expansivity 119×10^{-6} K^{-1} at 293 K is 2.42 J K^{-1} mol^{-1} in good agreement with the present result. The data of the bulk modulus and expansivity were taken from [9].

The experience leading to these results showed that there are a number of local minima in the parameter space if its dimension is large (e.g. 5). It is necessary to try various initial values to find the best solution for a given interpolation function. For a small number of the parameters (e.g. 3), the minimum found is likely to be the absolute minimum. This is especially true when the three parameters have distinct characters (Debye, Einstein and $C_p - C_v$ correction), as in the first model function for NaCl given above.

3.1. Sodium chloride with an artificial phase transition added to it

Having found that the quasi-harmonic heat capacity functions reproduce the heat capacity of sodium chloride in a wide temperature interval, we prepared an artificial set of data by adding the Ising mean-field heat capacity ($T_c = 100$ K) to the experimental values for sodium chloride. This simulated the heat capacity of a real compound that undergoes a phase transition. The data for 80–120 K were excluded (i.e. masked), because our aim was to test the fitting procedure's capability to find the correct normal heat capacity from a limited set of experimental data. The model function had four parameters (the Debye and Einstein temperatures, $C_p - C_v$ correction coefficient and the transition temperature) and converged quickly to the absolute minimum. The fitted result is shown in Fig. 3. The optimum parameter values are the Debye temperature 220.7 (0.5) K, Einstein temperature 260.4 (0.6) K, $A =$

Table 1
The molar heat capacity of NaCl ($R = 8.3145$ J K^{-1} mol^{-1})

T (K)	C_p(exp)/R	C_p(calc)/R
5.83	0.0026	0.0032
8.37	0.0084	0.0096
10.09	0.0155	0.0170
12.50	0.0316	0.0331
15.74	0.0697	0.0700
20.00	0.158	0.157
24.68	0.314	0.313
29.96	0.559	0.558
41.39	1.253	1.254
50.74	1.876	1.875
59.99	2.458	2.457
69.81	3.003	3.002
80.85	3.517	3.517
91.88	3.935	3.936
101.97	4.251	4.250
108.88	4.435	4.433
119.29	4.669	4.669
129.84	4.867	4.868
141.53	5.048	5.052
149.77	5.160	5.162
161.76	5.299	5.300
169.53	5.377	5.378
180.94	5.478	5.479
188.39	5.537	5.538
199.39	5.616	5.616
210.18	5.684	5.683
220.81	5.746	5.743
231.29	5.803	5.796
241.64	5.851	5.843
251.87	5.888	5.887
262.01	5.924	5.926
272.05	5.962	5.962
290.94	6.024	6.024
299.34	6.049	6.050
311.86	6.082	6.085

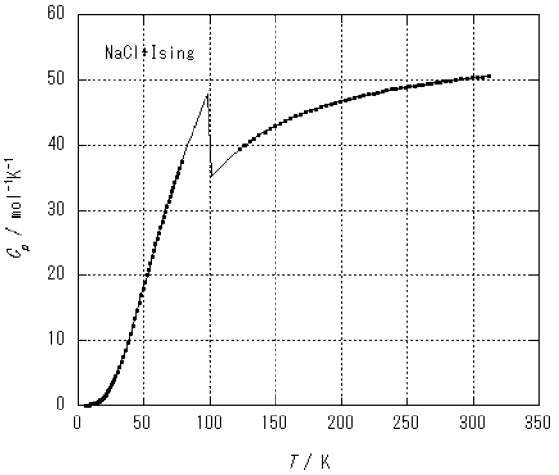

Fig. 3. The heat capacity of sodium chloride with an artificial Ising term added compared with the four-parameter fitting.

3.79 (0.03) $\times 10^{-6}$ mol J^{-1}, and T_c = 96.0 (0.3) K, the final χ^2 being 0.64 (J K^{-1} mol^{-1})^2 for 137 data points. The normal part is the same three-parameter function as the first of the two functions discussed in Section 2, where the best-fit parameters were 217.6 and 260.5 K for the Debye and Einstein temperatures and $A = 3.72 \times 10^{-6}$ mol J^{-1}. The best-fit values of the common parameters are satisfactorily close to each other. The transition temperature recovered is smaller than the supplied value by 4%. The difference is larger than we expected from the construction of the model, but may be accepted as a consequence of the limitation of the model function. For comparison, the best-fit result for the sodium chloride dataset masked in the interval 80–120 K (without an added Ising part) was 218.2 (0.5) and 259.4 (0.6) K, and 3.69 (0.03) $\times 10^{-6}$ mol J^{-1} for the Debye and Einstein temperatures, and the A coefficient, respectively, with the χ^2 value equal to 1.03 (J K^{-1} mol^{-1})^2.

In order to find how the result depends on the dataset, the program was run repeatedly on the dataset with the masked portion between 120 K and a increasingly lower temperature to 40 K. The Debye temperature was 221.8, 223.5, 226.5 and 231.7 K for the date set masked from 120 to 70, 60, 50, and 40 K, respectively. The best-fit values of the other parameters are as follows in the same order of the datasets: the Einstein temperature—260.3, 259.6, 257.9 and 254.6 K; the A coefficient—3.81 $\times 10^{-6}$, 3.82 $\times 10^{-6}$, 3.82 $\times 10^{-6}$ and 3.81 $\times 10^{-6}$ mol J^{-1}; T_c—95.1, 93.7, 91.4 and 85.9 K. There are weak systematic tendencies for the optimum parameter values to depend on the dataset. But we conclude the variation in the result is sufficiently small as long as a reasonably large magnitude of the excess heat capacity contributed in the low temperature phase. At 40 K, the phase transition contributes 1.6 J K^{-1} mol^{-1} to the heat capacity compared with the vibrational heat capacity of 12 J K^{-1} mol^{-1} at the same temperature. This small magnitude of the contribution from the phase transition explains the relative instability of the recovered transition temperature against the variation of the masked portion of the dataset.

3.2. Use of a polynomial function for the normal part

We may lack detailed knowledge about the heat capacity of the background thermal excitation. The present method is still applicable in such cases by the use of a polynomial in T for the normal part. This was shown on the same artificial data (i.e. sodium chloride + the Ising heat capacity with T_c = 100 K) as in Section 3.1. The fitting function employed was the sum of a third order polynomial and the Ising heat capacity. It was necessary to mask the data below 40 K and above 240 K as well as those between 80 and 120 K, because the polynomial function could not reproduce the experimental data in the same wide range of temperature as the harmonic heat capacity functions can. The central portion (80–120 K) was masked as it was for the fitting by the Debye and Einstein functions. The five-parameter fit converged uniquely. The recovered transition temperature was 90.2 K, not very far from the correct value.

4. Application to the gradual phase transition in tri-rubidium deuterium sulfate

The phase transition in tri-rubidium deuterium sulfate was reported by Gesi [10]. The phase transition and those occurring in the related compounds have been studied by X-ray diffraction [11], NMR [12–14], spectroscopic [15], neutron diffraction [16] and other methods. Interest in this phase transition centers around the fact that mere change of hydrogen

to deuterium results in the appearance of a different crystalline phase. Even the macroscopic symmetry of the crystal changes as a result of the increase of one molar mass unit in 450, though the symmetry of the low temperature phase has not been determined conclusively. If the transition entropy is close to $R\ln 2$, we can conclude that deuteron atoms are disordered in the high temperature phase and ordered in the low temperature phase, and hence the change of the crystal symmetry. This mechanism has a structural basis in the short hydrogen bond connecting two sulfate ions. For the hydrogenous crystal which does not undergo a phase transition, the proton on the hydrogen bond may be described as a proton cloud [17,18] because of its delocalization over two sites in the ground state.

The sample tri-rubidium hydrogen sulfate was prepared from aqueous solution of sulfuric acid and rubidium sulfate and recrystallized from aqueous solution by slow cooling. Single crystals of 0.5–10 mm size were obtained. TRDS was prepared from deuterated sulfuric acid, rubidium sulfate and D_2O. Deuteration was better than 99% from the proton concentration due to the starting materials. The chemical composition was checked by analysis for the sulfur content: 14.11% for TRHS and 14.14% for TRDS (with probable errors of 0.3%) in agreement with calculated values 14.27 and 14.23%, respectively.

Two adiabatic calorimeters I and II were used to cover the temperatures for 13–300 and 2–15 K. The sample masses were 8.7888 g (I) and 8.7678 g (II) for TRHS and 8.8801 g (I) and 8.8246 g (II) for TRDS.

4.1. Experimental results

The molar heat capacities are plotted in Fig. 4 for TRHS and TRDS. They are also given numerically in Tables 2 and 3. The heat capacity curves are obviously different from each other at the transition temperature. They are also different at low and high temperatures. At 30 K and below, the heat capacity of TRHS is larger than that of TRDS, while the relation is reversed above 200 K. The difference at higher temperature arises from the lower vibrational frequencies of deuterium than hydrogen, while the heat capacity difference at low temperature does not find an easy explanation. TRHS may be a convenient reference for estimation of the excess heat capacity of TRDS but

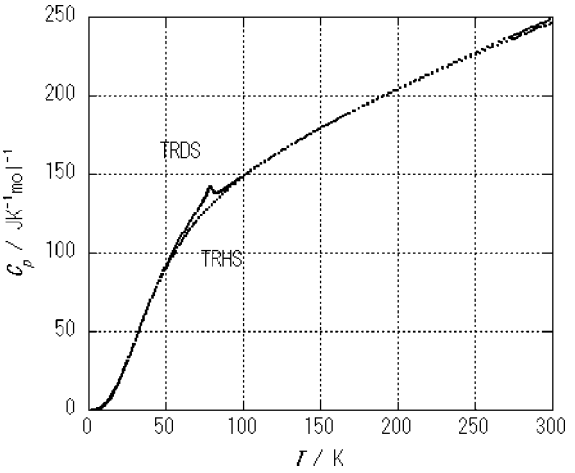

Fig. 4. The heat capacity of tri-rubidium hydrogen disulfate and tri-rubidium deuterium disulfate.

the reliability is limited by an uncertain contribution from the motion of hydrogen atom because the phase transition in TRDS occurs precisely as a result of this substitution.

4.2. Determination of the excess heat capacity of TRDS by least-squares fitting

There are 14 atoms in the chemical unit and hence 42 vibrational modes. Out of these, 18 are internal vibrations of the 2 sulfate ions. We measured the Raman spectrum and assigned the peaks following published data. They are O–S stretching modes at 1000–1200 cm^{-1} and O–S–O deformation modes at 440–620 cm^{-1}. We took these wave numbers to calculate the known Einstein temperatures listed in Table 4. Remaining 24 vibrations were determined by the extended least-squares. The interpolation function was: $\mathrm{Deb}(9)+\mathrm{Ein}(7)+\mathrm{Ein}(5)+\mathrm{Ein}(3)+(C_p-C_v)+\mathrm{Ising}$ with six adjustable parameters. The heat capacity data were masked between 72 and 175 K. The parameter values are given in Table 4. In Fig. 5, we plotted the heat capacity and its decomposition into contributions from the known internal vibrations of sulfate ions, optimized lattice vibrations of the anions, cations and deuterium atom, C_p-C_v correction and the excess part from the phase transition. The excess part is plotted in Fig. 6 where a significant magnitude at 40 K ($=T_c/2$) is notable. It has been possible to derive this part only

Table 2
The molar heat capacity of TRHS ($R = 8.3145\,\mathrm{J\,K^{-1}\,mol^{-1}}$)

T (K)	C_p/R	T (K)	C_p/R	T (K)	C_p/R	T (K)	C_p/R
2.34	0.00289	23.66	3.298	76.42	15.30	183.92	23.59
2.59	0.00371	24.48	3.544	78.06	15.51	186.88	23.75
2.74	0.00465	25.34	3.782	79.73	15.71	189.92	23.93
3.00	0.00538	26.22	4.053	81.40	15.91	192.96	24.10
3.02	0.00623	27.21	4.348	83.06	16.09	195.99	24.26
3.44	0.00809	28.31	4.717	84.76	16.29	199.02	24.46
3.60	0.00923	29.48	5.057	86.50	16.49	202.02	24.64
3.91	0.0119	30.66	5.416	88.10	16.65	205.02	24.80
4.19	0.0154	31.82	5.771	89.70	16.81	208.00	24.97
4.45	0.0194	32.97	6.125	91.96	17.04	210.98	25.13
4.78	0.0263	34.10	6.472	94.68	17.31	213.95	25.28
5.07	0.0294	35.18	6.795	97.28	17.55	216.91	25.46
5.35	0.0377	36.21	7.106	99.80	17.78	219.87	25.60
5.59	0.0439	37.24	7.405	102.28	18.01	222.90	25.76
5.86	0.0520	38.24	7.695	104.72	18.21	226.02	25.92
6.10	0.0597	39.27	7.987	107.13	18.42	229.13	26.10
6.37	0.0696	40.32	8.275	109.50	18.60	232.23	26.26
6.60	0.0791	41.34	8.556	111.84	18.80	235.33	26.41
6.85	0.0901	42.35	8.824	114.15	18.97	238.42	26.57
7.12	0.104	43.37	9.102	116.44	19.14	241.50	26.76
7.38	0.118	44.42	9.352	118.69	19.32	244.57	26.88
7.66	0.135	45.44	9.623	120.92	19.49	247.64	27.03
7.96	0.151	46.45	9.872	123.13	19.66	250.70	27.19
8.27	0.173	47.48	10.12	125.31	19.83	253.75	27.34
8.58	0.199	48.52	10.38	127.46	19.97	256.80	27.49
8.91	0.228	49.55	10.61	129.60	20.13	259.92	27.66
9.26	0.258	50.56	10.85	131.72	20.28	261.81	27.76
9.60	0.291	51.59	11.08	133.83	20.41	264.82	27.91
9.98	0.328	52.64	11.31	135.91	20.57	267.83	28.06
10.37	0.375	53.67	11.53	137.98	20.71	270.92	28.21
11.22	0.479	54.70	11.75	140.03	20.85	274.09	28.36
11.66	0.538	55.73	11.97	142.07	20.99	275.82	28.44
12.15	0.606	56.78	12.17	144.09	21.13	277.25	28.52
12.61	0.673	57.83	12.38	146.10	21.27	278.99	28.60
13.12	0.752	58.86	12.58	148.10	21.39	280.40	28.66
13.48	0.831	59.91	12.77	150.09	21.52	282.16	28.76
13.59	0.836	60.97	12.96	152.06	21.65	283.55	28.82
14.10	0.932	62.02	13.14	154.02	21.78	285.32	28.91
14.12	0.937	62.88	13.30	154.68	21.82	286.69	28.98
14.59	1.033	63.07	13.32	155.97	21.90	288.47	29.10
14.77	1.075	64.13	13.51	157.66	22.01	289.82	29.16
15.43	1.197	64.32	13.54	157.90	22.02	291.62	29.25
16.10	1.340	65.20	13.68	159.83	22.14	292.95	29.29
16.76	1.488	65.79	13.78	160.63	22.19	294.77	29.39
17.42	1.637	66.27	13.85	161.75	22.27	296.07	29.42
18.07	1.788	67.30	14.02	163.58	22.37	297.99	29.53
18.84	1.977	68.41	14.18	166.52	22.55	299.19	29.57
19.71	2.199	69.49	14.34	169.45	22.72	301.29	29.67
20.55	2.421	70.14	14.45	172.37	22.91	302.31	29.73
21.36	2.642	71.64	14.65	175.27	23.07		
22.14	2.862	73.24	14.89	178.16	23.25		
22.91	3.079	74.84	15.09	181.05	23.42		

Table 3
The molar heat capacity of TRDS ($R = 8.3145\,\mathrm{J\,K^{-1}\,mol^{-1}}$)

T (K)	C_p/R	T (K)	C_p/R	T (K)	C_p/R	T (K)	C_p/R
2.90	0.00470	37.64	7.559	79.79	16.93	123.10	19.66
2.97	0.00555	38.59	7.837	79.86	16.92	126.05	19.88
3.66	0.00870	39.51	8.109	80.20	16.87	128.99	20.09
3.86	0.0117	40.41	8.371	80.55	16.77	131.90	20.29
4.07	0.0126	41.33	8.636	80.75	16.75	134.80	20.50
4.33	0.0170	42.29	8.909	80.92	16.71	137.67	20.69
4.60	0.0208	43.22	9.166	81.30	16.66	140.62	20.89
4.94	0.0250	44.14	9.417	81.69	16.63	143.62	21.10
5.21	0.0314	45.04	9.672	81.72	16.61	146.62	21.29
5.53	0.0394	45.92	9.906	82.07	16.59	149.60	21.48
5.80	0.0446	46.82	10.15	82.46	16.58	152.64	21.68
6.10	0.0534	47.75	10.39	82.69	16.58	155.75	21.88
6.37	0.0615	48.67	10.62	82.85	16.58	158.85	22.08
6.69	0.0725	49.57	10.85	83.25	16.59	161.93	22.28
6.97	0.0834	50.46	11.08	83.64	16.59	165.07	22.48
7.28	0.0966	51.33	11.29	83.66	16.59	168.28	22.67
7.57	0.109	52.23	11.49	84.06	16.61	171.48	22.88
7.86	0.126	53.16	11.72	84.48	16.62	174.66	23.07
8.15	0.142	54.07	11.93	84.63	16.64	177.91	23.27
8.45	0.162	54.97	12.15	84.91	16.63	181.21	23.46
8.76	0.180	55.86	12.34	85.34	16.66	184.51	23.66
9.07	0.204	56.74	12.52	85.60	16.68	187.79	23.85
9.40	0.231	57.64	12.72	85.77	16.69	191.14	24.05
9.74	0.259	58.57	12.91	86.20	16.73	194.54	24.25
10.10	0.293	59.48	13.10	86.57	16.75	197.92	24.46
10.47	0.329	60.38	13.28	86.64	16.76	201.30	24.63
10.87	0.373	61.28	13.47	87.07	16.81	204.73	24.82
11.23	0.414	62.17	13.64	87.52	16.83	208.22	25.03
11.63	0.461	63.08	13.82	87.53	16.83	211.70	25.23
11.97	0.503	64.01	14.00	87.99	16.88	215.17	25.42
12.36	0.555	64.93	14.18	88.45	16.91	218.69	25.61
12.69	0.602	65.85	14.35	88.50	16.90	222.27	25.81
13.08	0.660	66.76	14.52	88.92	16.94	225.84	26.00
13.45	0.714	67.66	14.68	89.39	16.98	229.40	26.21
13.82	0.779	68.59	14.85	89.46	16.97	233.02	26.41
14.12	0.835	69.53	15.03	89.86	17.01	236.69	26.61
14.19	0.839	70.46	15.21	90.33	17.07	240.35	26.83
14.56	0.921	71.06	15.31	90.80	17.12	243.99	27.01
14.65	0.931	71.39	15.36	91.15	17.13	247.70	27.19
15.14	1.022	72.31	15.55	91.29	17.14	251.45	27.39
15.69	1.132	73.09	15.69	91.79	17.18	255.20	27.59
16.35	1.271	73.23	15.72	92.29	17.21	258.66	27.78
16.99	1.410	74.16	15.88	92.79	17.27	261.85	27.96
17.62	1.551	74.20	15.92	93.30	17.30	266.28	28.23
18.29	1.715	74.45	15.95	93.58	17.33	269.44	28.39
19.00	1.891	74.71	15.99	93.80	17.36	272.58	28.53
19.66	2.060	74.96	16.04	94.31	17.40	274.17	28.61
20.29	2.228	75.11	16.08	94.81	17.45	275.71	28.68
20.93	2.401	75.22	16.12	95.33	17.47	277.29	28.77
21.65	2.602	75.48	16.17	95.86	17.53	278.82	28.83
22.47	2.835	75.76	16.24	95.98	17.54	280.39	28.93
23.31	3.079	76.05	16.30	96.39	17.59	281.92	29.01
24.10	3.310	76.06	16.32	96.93	17.62	283.48	29.08

Table 3 (*Continued*)

T (K)	C_p/R	T (K)	C_p/R	T (K)	C_p/R	T (K)	C_p/R
24.85	3.533	76.35	16.36	98.34	17.74	285.01	29.16
25.63	3.768	76.64	16.45	98.40	17.75	286.56	29.24
26.49	4.030	76.94	16.52	100.66	17.94	288.08	29.33
27.30	4.283	76.99	16.56	100.75	17.95	289.62	29.42
28.10	4.540	77.24	16.63	102.96	18.12	291.14	29.48
28.94	4.822	77.54	16.74	103.05	18.14	292.67	29.55
29.78	5.078	77.85	16.85	105.22	18.30	294.18	29.59
30.67	5.357	77.92	16.89	105.32	18.32	295.71	29.70
31.60	5.653	78.17	16.95	107.55	18.50	297.21	29.75
32.58	5.968	78.50	17.06	109.77	18.67	298.74	29.86
33.59	6.288	78.83	17.06	111.96	18.84	300.24	29.92
34.62	6.612	78.84	17.05	114.49	19.03	301.76	30.01
35.66	6.944	79.17	17.03	117.35	19.25		
36.67	7.260	79.51	16.97	120.19	19.45		

by incorporating the adjustable transition contribution to the fitting function.

Other combinations of functions were also tried. Some did not converge, others converged but χ^2 was not sufficiently small and still others did reasonably well. The criterion of a good fit was small values of the χ^2 and small probable errors in the best-fit parameter values. The functional form was chosen by this criterion.

Table 4
Characteristic temperatures of TRDS

	Weight
From spectroscopy	
Einstein temperature (K)	
1451	2 (ν_1 of sulfate ion)
635	4 (ν_2 of sulfate ion)
1683	6 (ν_3 of sulfate ion)
879	6 (ν_4 of sulfate ion)
By fitting	
Einstein temperature (K)	
164.9 (1.4)	7
234.6 (5.7)	5
861.0 (16)	3
Debye temperature	
130.3 (0.4)	9
	42 (sum of the weights)
$C_p - C_v$ correction coefficient (mol J^{-1})	4.14 (0.17) $\times$ 10^{-7}
Mean-field transition temperature (K)	104.7 (4.7)

In lattice dynamic consideration, there is one acoustic branch for one primitive unit cell of the crystal and all the other branches are optical [19]. But the optical branch in which rubidium ions vibrate against each other is likely to have a wide band-width because of the mass equality. This consideration justifies the weight 9 of the Debye term. The $7+5$ Einstein terms may be related with rotational and translational vibrations of sulfate ions against each other and against rubidium ions, while the highest energy Einstein term may be identified with vibrations of the deuterium atom. For the last term, a higher energy (ca. 1100 K) is expected

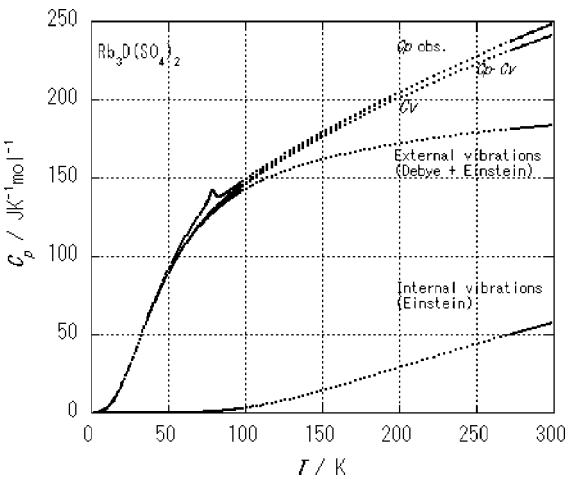

Fig. 5. Decomposition of the heat capacity of tri-rubidium deuterium disulfate into normal and transition contributions.

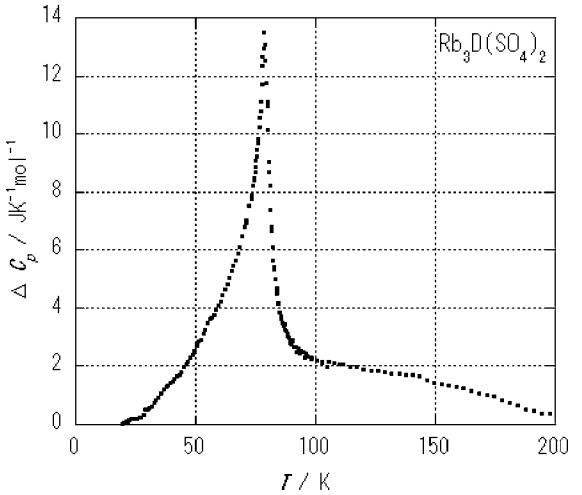

Fig. 6. The excess heat capacity of tri-rubidium deuterium disulfate.

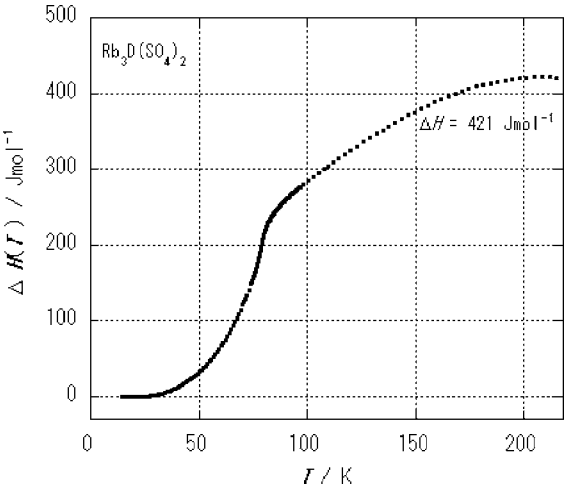

Fig. 7. The excess enthalpy of tri-rubidium deuterium disulfate.

from neutron data [20], but averaging over three modes (i.e. *x*, *y* and *z* vibrations) as well as general insensitivity of the heat capacity to high frequency modes may be responsible to the discrepancy. The weights 7 and 5 of the Einstein terms could be 6 and 6, but the present combination gave a smaller χ^2.

4.3. The transition enthalpy and entropy

The excess heat capacity was integrated with respect to T and $\ln T$ to determine the transition enthalpy and transition entropy, respectively. They are plotted in Figs. 7 and 8. The high temperature value of the enthalpy 421 J mol^{-1} is a measure of the stability of the low temperature phase in terms of the energy relative to the high temperature phase. The high temperature entropy 5.27 J K^{-1} mol^{-1} is related with structural disorder in the high temperature phase. The experimental value is sufficiently close to $R \ln 2 = 5.76$ J K^{-1} mol^{-1} to suggest that the high temperature phase is twofold disordered.

In the room temperature structure, the deuterium atom is located on the symmetry center between to sulfate ions. The present results shows that the center of symmetry is a result of disorder of the position of the deuterium. The deuterium bond lengths 0.2519 and 0.2533 nm appear to accommodate two stable positions for a deuterium between the two oxygen atoms in $K_3D(SO_4)_2$ [21] and $K_3D(SeO_4)_2$ [18], respectively. The transition enthalpy 421 J mol^{-1} may be identified with the energy of interaction between two neighboring deuterium bonds.

For the sake of comparison, we calculated the transition enthalpy and entropy by taking the heat capacity of TRHS as the normal heat capacity. For this, the heat capacity of TRHS was expressed in a fourth degree polynomial and subtracted from TRDS. The excess heat capacity was positive above 40 K and essentially zero above 120 K. The transition enthalpy

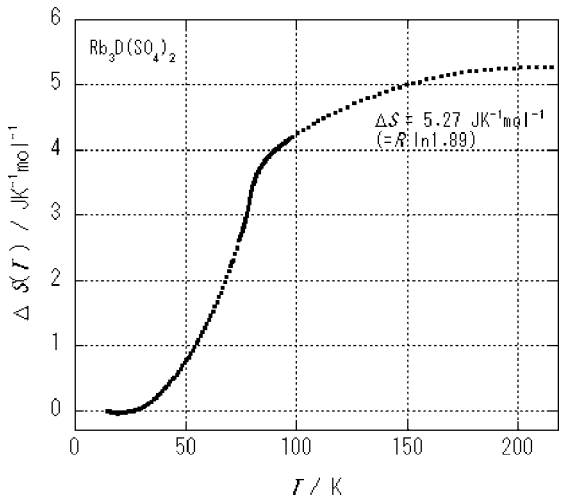

Fig. 8. The excess entropy of tri-rubidium deuterium disulfate.

and entropy $220\,J\,mol^{-1}$ and $3.19\,J\,K^{-1}\,mol^{-1}$, respectively, from this excess heat capacity are substantially smaller than those obtained by the extended least-squares fitting. Although the undeuterated compound lacking the phase transition is an obvious choice for the normal heat capacity, it is not the case for the present compounds: the heat capacity of TRHS is significantly larger than that of TRDS at low temperature (see further). It is likely that a small change in the lattice spectrum as a result of deuteration has changed the normal heat capacity of TRDS from the heat capacity of TRHS. A more interesting interpretation is to assume a tunnel state for the hydrogen atoms in TRHS. The heat capacity of TRHS then contains the contribution from the Schottky level. By taking TRHS as the reference, we have included this contribution in the normal part. The transition enthalpy and entropy of TRDS will be correspondingly smaller than is appropriate with proper evaluation of the phonon part. This explains what we have actually found. Attempts to determine the tunnel level by fitting the harmonic and Schottky heat capacities to the TRHS data converged easily, giving $\Delta E/R = 217\,K$ for the tunnel level using the data in the interval 7–80 K and a three-parameter harmonic fitting function. However, the result varied much with the interval and model functions.

4.4. The heat capacity of TRHS

The heat capacity of TRHS is a smooth function temperature between 2 and 300 K, proving the absence of a phase transition. It could be used as the base line for TRDS but not very successfully as described in Section 4.2. For the sake of comparison with TRDS, the best-fit function was $\mathrm{Deb}(9, \Theta_D = 124.5\,K) + \mathrm{Ein}(12, \Theta_E = 191.0\,K) + \mathrm{Ein}(3, \Theta_E = 752\,K)$ with the $C_p - C_v$ coefficient of $1.12 \times 10^{-7}\,mol\,J^{-1}$. Here again a higher Einstein temperature may be expected as with TRDS and the difference could be explained similarly.

4.5. The heat capacities at very low temperature

The heat capacity of TRHS is significantly larger than that of TRDS at temperatures between 2 and 30 K. This is unexpected because the mass effect suggests the opposite. As Fig. 9 shows, the difference amounts to $1.6\,J\,K^{-1}\,mol^{-1}$. The larger heat capacity

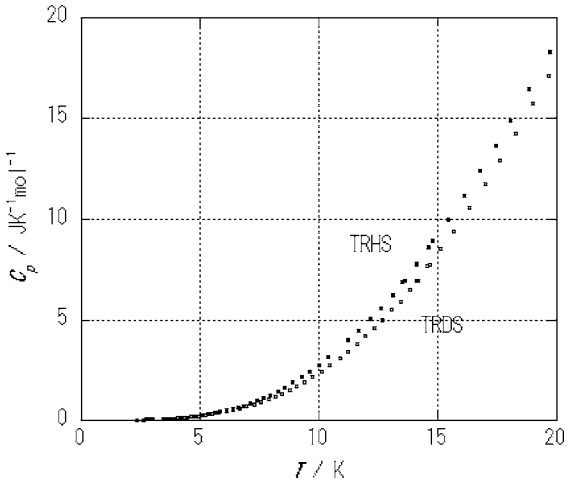

Fig. 9. The heat capacity of tri-rubidium hydrogen disulfate and tri-rubidium deuterium disulfate at low temperature.

of TRHS explains its failure as the normal heat capacity for TRDS. It could be attributed to a Schottky anomaly due to tunneling protons broadened by interaction between them, as proposed previously [22] for $Rb_3H(SeO_4)_2$. The inverse isotope effect where deuterated species has a smaller heat capacity than the normal one has been also found in NaOH–NaOD [23,24], the phenalenone derivatives [25,26] and several cubic ammonium compounds [27–30]. All of these substances share the property that they undergo phase transitions in the deuterated forms for which the structural aspect of the problem has also been studied [27,29].

5. Conclusion

In the present paper, we have shown a computational method to find the optimum parameter values for a given model of the heat capacity of solids that undergo phase transitions. The fitting procedure has eliminated a large part of arbitrary factors involved in the analysis of the heat capacity of gradual phase transitions. The method can be generalized in several directions. First, the fitting function can be made up of more than two pieces. In the cases discussed above we used different functions for low and high temperature regions. This can be generalized to three or more

regions with some parameters common among the regions. The Kaleidagraph mathematical functions allow this to be done easily. Second, the model functions can be generalized beyond those consisting of Debye and Einstein functions. We have shown explicitly that polynomial in temperature can be used for the normal heat capacity. It could be any calculable function of T. Similarly the equation for the extra contributions for particular fitting intervals can be freely chosen from a larger group of functions. The limit is set by the number (i.e. 9) of the parameters that can be dealt with by the Kaleidagraph fitting section. In practice the convergence is not assured, and even if the fitting has converged, the solution obtained may be a local minimum of χ^2. Probability of hitting a local minimum increases rapidly as the number of parameter increases. Within these obvious limitations associated with any non-linear least-squares fitting, the analysis presented here allows us to explore a greater number of possibilities of various physical models and to decide the good models on well-defined criteria.

The low temperature heat capacity has been the source of important knowledge about order and disorder and other thermal excitations in solids since early 1900 when helium gas was first liquefied. However, the only practical measures available for the analysis of the heat capacity have been to interpolate the normal heat capacity curve into an ill-defined transition interval by the use of a polynomial function in temperature. Modern commercial cryogenic calorimeters have broadened the scope of calorimetry to include novel compounds available only in a small quantity. The precision and accuracy of the measurement carefully conducted with the commercial instruments are sufficiently good for the data to be compared meaningfully with the Einstein, Debye and other theories of the heat capacity. The fitting method presented above should be useful in the analysis of the heat capacity obtained not only with the established adiabatic calorimeters as we have discussed above for TRDS and TRHS but also with those from the new generation of instruments.

Appendix A. The Debye function

The Debye heat capacity function was computed in the following forms:

- For $\Theta_D/T > 16$:

$$\mathrm{Deb}(\Theta_D, T) = 77.927\left(\frac{T}{\Theta_D}\right)^3. \quad \text{(A.1)}$$

- For $16 \geq \Theta_D/T > 6.7$:

$$\mathrm{Deb}(\Theta_D, T) = 0.59522 \Big/ \left(1+\left(\frac{(\Theta_D/T)-0.86335}{4.7573}\right)^{2.9489}\right). \quad \text{(A.2)}$$

Table B.1
Standard thermodynamic functions of NaCl ($R = 8.3145\ \mathrm{J\,K^{-1}\,mol^{-1}}$)

T (K)	C_p°/R	H°/RT	S°/R	$(S^\circ/R) - (H^\circ/RT)$
5	0.00147	0.00034	0.00044	0.00010
10	0.0151	0.00346	0.00448	0.00103
15	0.0589	0.0135	0.0175	0.00402
20	0.158	0.0360	0.0466	0.0106
25	0.327	0.0761	0.0987	0.0226
30	0.561	0.1365	0.1780	0.0415
40	1.161	0.3149	0.4185	0.1035
50	1.827	0.5507	0.7490	0.1983
60	2.458	0.817	1.139	0.3220
70	3.011	1.092	1.560	0.4685
80	3.479	1.362	1.994	0.6321
90	3.870	1.620	2.427	0.8075
100	4.195	1.861	2.852	0.9908
110	4.462	2.086	3.265	1.179
120	4.683	2.294	3.663	1.369
130	4.869	2.485	4.045	1.561
140	5.029	2.661	4.412	1.751
150	5.162	2.823	4.764	1.941
160	5.285	2.973	5.101	2.127
170	5.382	3.112	5.424	2.312
180	5.470	3.241	5.734	2.494
190	5.548	3.360	6.032	2.672
200	5.619	3.471	6.319	2.847
210	5.684	3.575	6.594	3.019
220	5.742	3.672	6.860	3.188
230	5.794	3.763	7.116	3.353
240	5.840	3.849	7.364	3.515
250	5.881	3.929	7.603	3.674
260	5.919	4.005	7.835	3.829
270	5.954	4.077	8.059	3.982
273.15	5.965	4.098	8.128	4.029
280	5.988	4.144	8.276	4.131
290	6.020	4.209	8.486	4.278
298.15	6.045	4.258	8.654	4.395
300	6.050	4.269	8.691	4.422
310	6.078	4.327	8.890	4.563
320	6.103	4.382	9.083	4.701

- For $6.7 \geq \Theta_D/T$:

$$\mathrm{Deb}(\Theta_D, T) = 0.62663 \exp\left(-\left(\frac{\Theta_D/T}{3.5621}\right)^{1.9922}\right) + \frac{0.37341}{1 + ((\Theta_D/T)/6.8099)^{3.5919}}. \quad \text{(A.3)}$$

Here the Debye function with the characteristic temperature Θ_D is normalized to 1 in the high temperature limit. The numbers in these functions have been determined by the least-squares fitting to reproduce the Debye function to 0.02% for most of the temperatures relevant to the present purpose.

Table B.2
Standard thermodynamic functions of TRHS ($R = 8.3145\,\mathrm{J\,K^{-1}\,mol^{-1}}$)

T (K)	C_p°/R	H°/RT	S°/R	$(S^\circ/R) - (H^\circ/RT)$
5	0.0292	0.0069	0.0088	0.0019
10	0.333	0.0760	0.0972	0.0212
15	1.116	0.2789	0.3637	0.0848
20	2.278	0.6274	0.8365	0.2091
25	3.682	1.095	1.492	0.3972
30	5.213	1.653	2.298	0.6448
35	6.753	2.272	3.217	0.9454
40	8.186	2.923	4.214	1.291
45	9.522	3.583	5.257	1.673
50	10.73	4.238	6.323	2.085
55	11.81	4.878	7.397	2.519
60	12.78	5.497	8.467	2.970
65	13.65	6.091	9.525	3.434
70	14.42	6.659	10.57	3.906
75	15.12	7.200	11.58	4.384
80	15.75	7.715	12.58	4.866
85	16.32	8.205	13.55	5.348
90	16.84	8.670	14.50	5.830
95	17.33	9.113	15.42	6.311
100	17.80	9.536	16.33	6.789
110	18.64	10.33	18.06	7.736
120	19.40	11.05	19.72	8.666
130	20.13	11.72	21.30	9.577
140	20.83	12.35	22.82	10.47
150	21.51	12.94	24.28	11.34
160	22.15	13.49	25.69	12.19
170	22.78	14.02	27.05	13.03
180	23.38	14.52	28.37	13.84
190	23.96	15.01	29.65	14.64
200	24.53	15.47	30.89	15.42
210	25.07	15.91	32.10	16.19
220	25.61	16.34	33.28	16.94
230	26.13	16.76	34.43	17.68
240	26.65	17.16	35.55	18.40
250	27.15	17.55	36.65	19.11
260	27.65	17.93	37.73	19.80
270	28.15	18.30	38.78	20.48
273.15	28.31	18.41	39.11	20.70
280	28.65	18.66	39.81	21.16
290	29.14	19.01	40.83	21.82
298.15	29.55	19.29	41.64	22.35
300	29.64	19.36	41.82	22.47

Table B.3
Standard thermodynamic functions of TRDS ($R = 8.3145\,\mathrm{J\,K^{-1}\,mol^{-1}}$)

T (K)	C_p°/R	H°/RT	S°/R	$(S^\circ/R) - (H^\circ/RT)$
5	0.0268	0.0066	0.0084	0.0019
10	0.2834	0.0655	0.0845	0.0190
15	1.003	0.2444	0.3183	0.0740
20	2.147	0.5701	0.7552	0.1851
25	3.571	1.024	1.383	0.3587
30	5.148	1.579	2.172	0.5930
35	6.747	2.204	3.086	0.8825
40	8.242	2.867	4.086	1.220
45	9.671	3.544	5.141	1.596
50	10.96	4.223	6.228	2.005
55	12.13	4.889	7.328	2.439
60	13.20	5.538	8.430	2.892
65	14.19	6.166	9.526	3.360
70	15.13	6.773	10.61	3.840
75	16.06	7.360	11.69	4.327
80	16.89	7.941	12.76	4.821
85	16.65	8.453	13.77	5.318
90	17.03	8.919	14.73	5.815
95	17.46	9.358	15.67	6.309
100	17.87	9.773	16.57	6.799
110	18.66	10.55	18.31	7.768
120	19.41	11.25	19.97	8.716
130	20.14	11.91	21.55	9.643
140	20.84	12.52	23.07	10.55
150	21.51	13.10	24.53	11.43
160	22.17	13.65	25.94	12.30
170	22.80	14.17	27.30	13.14
180	23.41	14.66	28.62	13.96
190	24.00	15.14	29.91	14.77
200	24.58	15.60	31.15	15.56
210	25.15	16.04	32.36	16.33
220	25.70	16.46	33.55	17.08
230	26.24	16.88	34.70	17.82
240	26.78	17.28	35.83	18.55
250	27.31	17.67	36.93	19.26
260	27.84	18.05	38.01	19.96
270	28.36	18.42	39.08	20.65
273.15	28.53	18.54	39.41	20.87
280	28.89	18.79	40.12	21.33
290	29.42	19.14	41.14	22.00
298.15	29.90	19.43	41.96	22.53
300	29.95	19.50	42.15	22.65

Appendix B. Thermodynamic functions

The thermodynamic functions of sodium chloride (Table B.1), tri-rubidium hydrogen disulfate (Table B.2) and tri-rubidium deuterium disulfate (Table B.3) calculated from the heat capacity data are given in the dimensionless form.

References

[1] T. Matsuo, N. Kinami, H. Suga, Thermochim. Acta 267 (1995) 421–434.
[2] M. Uetani, O. Yamamuro, A. Inaba, T. Matsuo, M. Ichikawa, J. Korean Phys. Soc. 32 (1998) S397.
[3] T. Matsuo, S. Baluja, Y. Koike, M. Ohama, T. Mochida, T. Sugawara, Chem. Phys. Lett. 342 (2001) 22.
[4] K. Gesi, J. Phys. Soc. Jpn. 48 (1980) 886.
[5] R.H. Brout, Phase Transitions, Benjamin, New York, 1965 (Chapter 2).
[6] K. Clusius, J. Goldmann, A. Perlick, Z. Naturforsch. 4a (1949) 424.
[7] J.A. Morrison, D. Patterson, J.S. Dugdale, Can. J. Chem. 33 (1955) 375.
[8] T. Matsuo, K. Kohno, A. Inaba, T. Mochida, A. Izuoka, T. Sugawara, J. Chem. Phys. 108 (1998) 9809–9816.
[9] T.H.K. Barron, G.K. White, Heat Capacity and Thermal Expansion at Low Temperatures, Kluwer Academic Publishers/Plenum Press, New York, 1999, 153 pp.
[10] K. Gesi, J. Phys. Soc. Jpn. 61 (1992) 162.
[11] M. Ichikawa, Ferroelectrics 168 (1995) 177.
[12] U. Mikac, D. Arcon, B. Zalar, J. Dolinsek, R. Blinc, Phys. Rev. B 59 (1999) 11293.
[13] S. Takeda, F. Kondoh, N. Nakamura, K. Yamaguchi, Physica B 226 (1996) 157.
[14] A. Titze, G. Hinze, R. Boehmer, Phys. Rev. B 57 (1998) R666.
[15] P. Kaung, M. Kasahara, T. Yagi, J. Phys. Soc. Jpn. 65 (1996) 1114.
[16] R. Melzer, R. Sontag, K.S. Knight, Acta Crystallogr. C 62 (1996) 1062.
[17] T. Matsuo, A. Inaba, O. Yamamuro, N. Onoda-Yamamuro, J. Phys. Condens. Matter 12 (2000) 8595.
[18] N. Onoda-Yamamuro, O. Yamamuro, T. Matsuo, M. Ichikawa, R.M. Ibberson, W.I.F. David, J. Phys. Condens. Matter 12 (2000) 8559.
[19] A.A. Maradudin, E.W. Montroll, G.H. Weiss, Theory of Lattice Dynamics in the Harmonic Approximation, Academic Press, New York, 1964 (Chapter 1).
[20] F. Fillaux, A. Lautie, J. Tomkinson, G.J. Kearley, Chem. Phys. 154 (1991) 135.
[21] Y. Noda, H. Kasatani, Y. Watanabe, H. Terauchi, K. Gesi, J. Phys. Soc. Jpn. 59 (1994) 3249.
[22] M. Fukai, A. Inaba, T. Matsuo, H. Suga, M. Ichikawa, Solid State Commun. 87 (1993) 939.
[23] M.A. White, S.A. Moore, J. Chem. Phys. 85 (1986) 4629.
[24] P.W.R. Bessonette, M.A. White, J. Chem. Phys. 110 (1999) 3919.
[25] T. Matsuo, K. Kohno, A. Inaba, T. Mochida, A. Izuoka, T. Sugawara, J. Chem. Phys. 108 (1998) 9809.
[26] T. Matsuo, K. Kohno, M. Ohama, T. Mochida, A. Izuoka, T. Sugawara, Europhys. Lett. 47 (1999) 36.
[27] Y. Kume, Y. Miyazaki, T. Matsuo, H. Suga, W.I.F. David, R.M. Ibberson, Europhys. Lett. 16 (1991) 265.
[28] Y. Kume, Y. Miyazaki, T. Matsuo, H. Suga, J. Phys. Chem. Solids 53 (1992) 1297.
[29] Y. Kume, Y. Miyazaki, T. Matsuo, H. Suga, W.I.F. David, R.M. Ibberson, Physica B 180–181 (1992) 594.
[30] Y. Kume, H. Muraoka, O. Yamamuro, T. Matsuo, J. Chem. Phys. 108 (1998) 4090.